Molecular states in the equator-equator orientation of two oblately deformed ^{12}C nuclei

Jürgen Schmidt* and Werner Scheid
Institut für Theoretische Physik der Justus-Liebig-Universität, D-35392 Giessen, Germany
and Instituto de Ciencias Nucleares, Universidad Nacional Autónoma de México, México D.F., México
(Received 18 May 1995)

Intermediate resonance states in the $^{12}C + ^{12}C$ system are explained in the framework of a phenomenological model assuming the oblately deformed ^{12}C in the equator-equator orientation. The corresponding internuclear potential is determined by means of a double-folding model with parameters obtained by an optical model calculation reproducing the experimental excitation function. With this potential energy expanded around the stable equator-equator orientation, the Schrödinger equation is approximately solved. The obtained energies of the eigenstates are compared with experimental data and their decay widths are calculated.

PACS number(s): 25.70.Ef, 24.10.Ht, 24.30.Gd

I. INTRODUCTION

After the discovery of narrow resonance structures in the low energy scattering of two ^{12}C nuclei by Bromley *et al.* [1] selected heavier systems, like $^{12}C + ^{16}O$ [2], $^{24}Mg + ^{24}Mg$ [3], and $^{28}Si + ^{28}Si$ [4], have also revealed small resonance widths at higher angular momenta. The main common attributes are the high correlation of resonances between different exit channels, the appearance of several resonances per grazing partial wave, and the preference of those channels which approximately conserve the identity of the scattering partners. Since statistical analyses have not been able to explain these resonances as compound nucleus fluctuations (see, e.g., [5,6]), one has postulated a molecular origin. Molecular models presupposing dinuclear configurations have been successfully applied to these systems [7], e.g., to the $^{24}Mg + ^{24}Mg$ system by Uegaki and Abe [8,9] and by Maass and Scheid [10–12]. These authors consider various but different excitation modes with respect to the favored equilibrium configuration where the nuclei touch each other with their poles. As a result both models reproduce roughly the level density and distribution of decay widths.

Coupled channel (CC) calculations usually use a restricted number of molecular states built up by the states of the separated nuclei. They cannot reproduce the experimental decay widths of $^{24}Mg + ^{24}Mg$ scattering [11]. In the case of the lighter $^{12}C + ^{12}C$ system coupled channel calculations give uncorrelated resonance structure with nearly correct widths above $E_{\mathrm{c.m.}} = 10$ MeV [13]. The resonances in the region of $E_{\mathrm{c.m.}} < 10$ MeV, which have very small experimental widths, are not reproduced. Thus the question arises whether our molecular model of the $^{24}Mg + ^{24}Mg$ system can explain the intermediate resonances of the well investigated $^{12}C + ^{12}C$ system, too. The aim of the present paper is the study of the resonance states formed by two oblate ^{12}C nuclei in molecular configurations. Similar investigations have been recently published by Uegaki and Abe [14] for the $^{28}Si + ^{28}Si$ as an example of an oblate-oblate dinuclear system. The development of their model on the $^{28}Si + ^{28}Si$ system was carried out parallel to our work on the $^{12}C + ^{12}C$ system [15].

In our approach, we first make a phenomenological ansatz for the potential energy by means of the double-folding model using the sudden approximation for convenience. The parameters of the potential are determined in such a way that an optical model calculation reproduces roughly the experimental gross structure of the excitation function of $^{12}C + ^{12}C$. Starting with a general Hamiltonian for the two cluster system, we look for quasibound states in the equator-equator (EE) orientation of the oblately deformed ^{12}C nuclei. By introducing approximations similar to those of Ref. [11] we calculate spectra of resonances and the decay widths into various ^{12}C channels.

In Sec. II the basic Hamiltonian is explained. The calculation of the internuclear potential is shown in Sec. III including the optical model calculation and the application to the nuclear molecule. Finally, Sec. IV gives the approximate calculation of molecular resonances and decay widths.

II. THE COLLECTIVE HAMILTONIAN

In coupled channel calculations for elastic and inelastic scattering, the Hamiltonian describing the radial motion and the intrinsic structure of the nuclei can be written in the molecular c.m. frame (primed coordinates, $\boldsymbol{r} = r\boldsymbol{e}_{z'}$) as follows:

$$H_{\mathrm{CC}} = \frac{p_r^2}{2\mu} + \frac{(\boldsymbol{I}-\boldsymbol{J}_1-\boldsymbol{J}_2)_{x'}^2 + (\boldsymbol{I}-\boldsymbol{J}_1-\boldsymbol{J}_2)_{y'}^2}{2\mu r^2} + \sum_{i=1}^{2} T_{\mathrm{RVM}}(\boldsymbol{J}_i, \beta_i, \gamma_i) + U(r, \beta_1, \gamma_1, \Omega_1', \beta_2, \gamma_2, \Omega_2') + iW + \sum_{i=1}^{2} \left(\frac{C_\beta}{2}(\beta_i \cos\gamma_i - \beta_0)^2 + \frac{C_\gamma}{2}(\beta_i \sin\gamma_i)^2 \right). \tag{1}$$

Here, $\boldsymbol{I}$ denotes the total angular momentum and $\boldsymbol{J}_1$ and $\boldsymbol{J}_2$ are the intrinsic spins. T_{RVM} means the kinetic energy operator of the rotation-vibration model (RVM) [16]. The Euler

*Present address: Mathematisches Institut der Justus-Liebig-Universität, D35392 Giessen, Germany.

angles $\Omega_i'=(\varphi_i',\vartheta_i',\psi_i')$ $(i=1,2)$ describe the orientation of each nucleus with respect to the molecular (MO) frame. β_i and γ_i $(i=1,2)$ are the intrinsic quadrupole deformation coordinates. The potential U depends on the deformation and orientation of the nuclei and can be written as

$$U(r,\beta_1,\gamma_1,\Omega_1',\beta_2,\gamma_2,\Omega_2') = V(r)+V_{\text{coupl}}(r,\beta_1,\gamma_1,\Omega_1',\beta_2,\gamma_2,\Omega_2'). \quad (2)$$

The potential $V+iW$ is the r-dependent optical potential. V_{coupl} can be expanded in a series of spherical harmonics and deformation coordinates in the c.m. frame with space-fixed axes (subsequent use of the notation ''c.m. frame'' refers to such a coordinate system) in which CC calculations are performed usually. Likewise, the required wave functions can be expanded in an asymptotic basis (channel wave functions) which couple in the region of interaction.

First, we use the optical model for the determination of the potential parameters by reproducing the gross structure in the $^{12}C + {}^{12}C$ elastic 90° differential cross section. On the other hand, we construct quasibound states with the same Hamiltonian but in the MO frame by using appropriate approximations. It is possible to combine both studies in one picture by expanding the wave function in a series of both the channel wave functions and the molecular quasibound states [12]. Cross sections can be obtained either by means of an extended CC calculation or by using the R-matrix theory with several approximations. In the latter case the narrow resonances appear as Breit-Wigner resonance terms added to the S matrix of the conventional CC calculation.

III. THE NUCLEUS-NUCLEUS POTENTIAL

A potential depending on the geometrical properties of the nuclei is required. As nuclear molecules have longer lifetimes, they can be treated adiabatically, which is a difficult task [10]. A new ansatz for calculating an adiabatic potential is the symplectic model where a microscopic Hamiltonian is mapped onto a phenomenological potential. For molecular potentials a procedure of interpolation between the composite system and the separated nuclei is applied [17].

Another possibility is the double-folding model which we have chosen here for reasons of simplicity. In combination with the sudden approximation the potential is a function of the collective coordinates as requested. In this case the individual nuclear densities are added in the region of overlap. Special care has to be taken when the radial distance becomes too small. Actually this approximation is only adequate in high energy collisions, but has been successfully applied, e.g., by Uegaki and Abe [8]. We use the following nucleon-nucleon interaction:

$$v(\boldsymbol{r},\rho)=[V_a\exp(-r/\mu_a)/r+V_r\exp(-r/\mu_r)/r]\times\exp(-\gamma\rho)+V_p\delta(r)+V_{\text{Coulomb}}. \quad (3)$$

The genuinely nuclear part is a sum of an attractive and repulsive Yukawa potential which is density dependent in a simple way. The advantage of such a dependence appears in a shallower potential without softening the barrier step (cf. Ref. [18]). In order to describe greater overlaps of the nuclei more accurately, we have added a repulsive delta interaction potential (cf. Ref. [8]). Thus the more the nuclei overlap, the greater the repulsion of this pseudopotential becomes which can be interpreted as caused by the Pauli principle.

The ranges of the Yukawa forces refer to the values of the M3Y interaction [18], i.e., $\mu_a=0.45$ fm and $\mu_r=0.25$ fm. The strength parameters are determined via a scattering calculation presented in the next section with the result $V_a=-780$ MeV fm, $V_r=1460$ MeV fm, and $V_p=25$ MeV fm^3. Moreover, we have used $\gamma=5.4$ fm^3.

The folding potential in the sudden approximation $(\rho=\rho_1+\rho_2)$ is defined in the c.m. frame as

$$U(\boldsymbol{r},\alpha_\mu^{(1)},\alpha_\mu^{(2)})=\int\int d^3r_1d^3r_2\rho_1(\boldsymbol{r}_1,\alpha_\mu^{(1)})\times v(\boldsymbol{r}+\boldsymbol{r}_1-\boldsymbol{r}_2,\rho)\rho_2(\boldsymbol{r}_2,\alpha_\mu^{(2)}). \quad (4)$$

Here $\alpha_\mu^{(i)}$ are intrinsic quadrupole deformation coordinates in the c.m. frame. Using the techniques of Fourier transformation and transforming the potential into the MO frame we obtain by a straightforward calculation (see, e.g., Ref. [18])

$$U(r,\beta_1,\varphi_1',\vartheta_1',\beta_2,\varphi_2',\vartheta_2')=\sum_{\substack{l_1l_2m\\ m\geqslant 0}} U^m_{l_1l_2}(r,\beta_1,\beta_2)\cos[m(\varphi_2'-\varphi_1')]P^m_{l_1}(\cos\vartheta_1')P^m_{l_2}(\cos\vartheta_2'), \quad (5)$$

with

$$U^m_{l_1l_2}(r,\beta_1,\beta_2)=\sum_l \frac{2}{\pi} i^{l+l_1-l_2}(2l_1+1)^{1/2}(2l_2+1)^{1/2}(l_10l_20|l0)\int_0^\infty dk k^2 A^{(1)}_{l_10}(k,\beta_1)A^{(2)}_{l_20}(k,\beta_2)\tilde{v}(k)j_l(kr)(-)^m \times(l_1ml_2-m|l0)(2-\delta_{m0})[(l_1-m)!(l_2-m)!]^{1/2}[(l_1+m)!(l_2+m)!]^{-1/2}. \quad (6)$$

$P_l^m(x)$ denotes the Legendre polynomial, $j_l(kr)$ are spherical Bessel functions, and $\tilde{v}(k)$ is the Fourier transform of the nucleon-nucleon interaction. Note that Eq. (5) merely describes nuclei with axial symmetry around the intrinsic axes, i.e., with β deformations. Only the so-called form factors depend on the deformation of each nucleus ($i=1,2$; double primed coordinates: intrinsic principle-axes system):

$$A_{l0}^{(i)}(k,\beta_i)=2\pi\int_0^\infty dr_i''r_i''^2 j_l(kr_i'')\int_0^\pi d\vartheta_i''\sin\vartheta_i''\rho_i \times\exp(-\gamma\rho_i)Y_{l0}(\vartheta_i''). \quad (7)$$

For calculating the density dependent part of the interaction given in Eq. (3) we set $\exp(-\gamma\rho)=\exp(-\gamma\rho_1)\exp(-\gamma\rho_2)$ as usual [19]. This density dependence causes a factor $\rho_i\exp(-\gamma\rho_i)$ without requiring additional effort.

A single ^{12}C nucleus in its ground state can be satisfactorily described as solely β deformed [20]. Although γ deformation could be important for the description of the nucleus as a molecular constituent part, we neglect this deformation here for convenience. Since different ground state deformations have been measured with several methods (see, e.g., Refs. [20,21]), we have assumed a mean value of $\beta_0=-0.60$. Moreover, a nuclear Fermi density distribution ($i=1,2$)

$$\rho(r_i'',\vartheta_i'',\beta_i)=\rho_0(1+\exp\{[r_i''-R(\vartheta_i'',\beta_i)]/a\})^{-1} \quad (8)$$

with

$$R(\vartheta_i'',\beta_i)=R_0(\beta_i)[1+\beta_i Y_{20}(\vartheta_i'')] \quad (9)$$

has been fitted to twice the experimental proton density distribution [22], with β_i being zero. We have chosen $\rho_0=0.18$ fm^{-3} and $a=0.55$ fm. With these variables kept fixed, $R_0(\beta_i)$ is determined in such a way that the condition of mass conservation is fulfilled for each value of β_i.

The form factors $A_{l0}^{(i)}$ with $l>2$ can be neglected due to their very small contributions. The coefficients $U_{l_1l_2}^m(r,\beta_1,\beta_2)$ have been calculated by means of a Gauss-Legendre integration.

A. Optical model calculations

In this calculation we do not consider inelastic channels. $U_{00}^0(r,\beta_1=\beta_2=0)$ is used as a real part of the optical potential $V(r)$. By following the statistical model of Helling *et al.* [23] the imaginary potential can be written as

$$W(r,E,I)=\alpha N(r)\frac{2I+1}{\sigma^3} \times\exp\left\{2\sqrt{a[E-V(r)]}-\frac{(I+1/2)^2}{2\sigma^2}\right\}, \quad (10)$$

with

$$\sigma^2=\frac{\Theta_{\rm cl}(r)}{\hbar^2}\left(\frac{E-V(r)}{\beta}\right)^{1/2}, \quad \Theta_{\rm cl}(r)=\mu\left(\frac{8}{5}R_0^2+r^2\right). \quad (11)$$

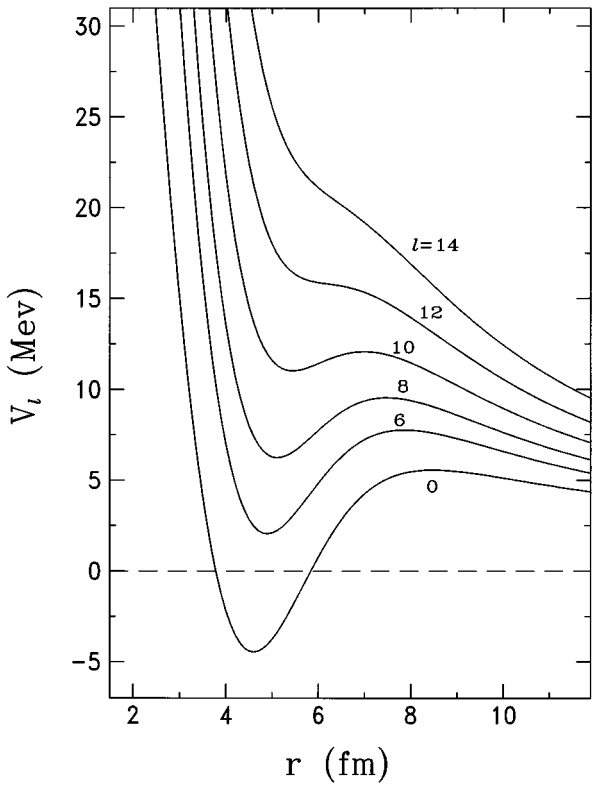

FIG. 1. Potentials $V_l(r)=V_0(r)[=U_{00}^0(r,\beta_1=\beta_2=0)]+\ell(\ell+1)\hbar^2/(2\mu r^2)$ for various angular momenta.

Here $\Theta_{\rm cl}(r)$ is the classical moment of inertia and σ is a spin cutoff parameter. The parameter α determines the absorption strength and β adjusts the angular momentum dependence of W. Since the absorption mainly occurs at the touching region of the nuclei, the radial function $N(r)$ is chosen as a Woods-Saxon form (radius and diffuseness parameters $2R_0$ and $\tilde{\gamma}$, respectively) rather than the number of nucleons in the overlap region (cf. Ref. [11]). The strength of $N(r)$ is set 12 for the sake of equivalence to the usual function at $r=0$.

As the calculations of Korotky [24] have been very successful in describing the experimental excitation function, we have first tried to reproduce the virtual resonance energies of the Korotky potential by performing calculations without an absorptive potential. So the real part of the potential $V(r)$ has been fixed (for parameters see above) with resonance energies 8.9, 12.8, 17.5, 23.6, and 31.1 MeV for the angular momenta $l=8$, 10, 12, 14, and 16, respectively. The obtained potential $V(r)$ is shown in Fig. 1 where also the centrifugal potentials are added. Then the calculated elastic 90° differential cross section has been fitted to the experimental one by varying α, β, and $\tilde{\gamma}$. Best results have been obtained with $\alpha=-0.07$ MeV, $\beta=0.31$ MeV^{-1}, and $\tilde{\gamma}=0.55$ fm, the radius $R_0=3.11$ fm being used. Evidently the gross structures of the excitation function are well reproduced as shown in Fig. 2.

B. The molecular potential for several orientations

In Sec. IV we will use the potential energy Eq. (5) in order to obtain the quasibound states of the Schrödinger equation. Since the rotational energy influences the properties of the potential minima, around which the quasibound

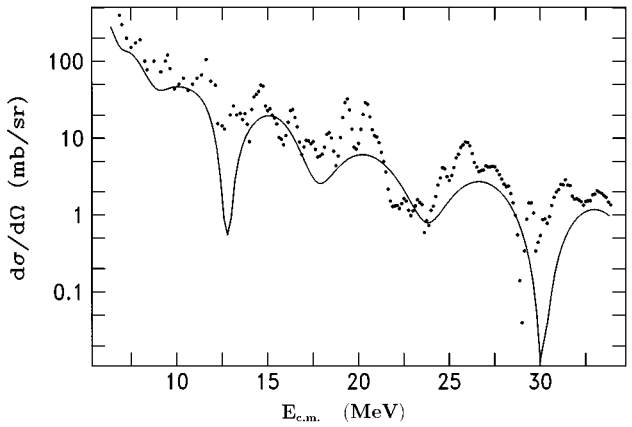

FIG. 2. Elastic excitation function ($\vartheta_{\mathrm{c.m.}}=90°$) for the scattering of ^{12}C on ^{12}C calculated with the potentials of Fig. 1. The dots are experimental values taken from [24].

states are situated, this energy should be chosen very carefully. As an approximation we assume a stiff rotation of the whole molecule, which means ''frozen'' intrinsic degrees of freedom, rather than neglecting individual rotations [11]. Therefore, the Hamiltonian for calculating effective potentials reads

$$H^I_{\mathrm{PES}}=\frac{1}{2}\boldsymbol{I}'^{\,t}\Theta^{-1}\boldsymbol{I}'+U(r,\beta_1,\varphi_1',\vartheta_1',\beta_2,\varphi_2',\vartheta_2') + \sum_{i=1}^{2}\frac{C_\beta}{2}(\beta_i-\beta_0)^2, \tag{12}$$

with $r,\beta_1,\beta_2,\vartheta_1',\vartheta_2'$, and $(\varphi_2'-\varphi_1')$ fixed. $\boldsymbol{I}'$ is the operator of the total angular momentum and Θ is the inertia tensor, both with respect to the axes of the MO system. Θ is a sum of the diagonal inertia tensor of the relative motion Θ_r and the inertia tensors of each nucleus Θ_i $(i=1,2)$. The latter can be obtained by means of the transformation $\Theta_i=R_i^t(\Omega_i')\tilde{\Theta}_i R_i(\Omega_i')$ [15,16] with

$$\tilde{\Theta}_i=\begin{pmatrix} 3B_0\beta_i^2 & 0 & 0\\ 0 & 3B_0\beta_i^2 & 0\\ 0 & 0 & 0\end{pmatrix}. \tag{13}$$

Using the value of $\beta_0=-0.60$ we have calculated $C_\beta=36.6$ MeV and $B_0=0.626\hbar^2$ MeV^{-1} according to the RVM [16].

First, we diagonalize Θ for arbitrary but fixed orientations of the nuclei, i.e., we transform to a molecular principle-axes system. Then Eq. (12) describes a triaxial rotator and the corresponding Schrödinger equation is solved by diagonalization in the eigenstates of the symmetric rotator $|IMK\rangle$ [cf. asymmetric rotator model (ARM) [16]]. Note that only even K values appear here because of the unambiguousness of the wave function. In case that the intrinsic symmetries of the molecule are considered, too, odd K values are consequently allowed (see Sec. IV). That is why our calculation of the effective potential has an approximate character.

Figure 3 shows the radial intersections of the potential energy surface (PES) for three orientations of the axes, i.e.,

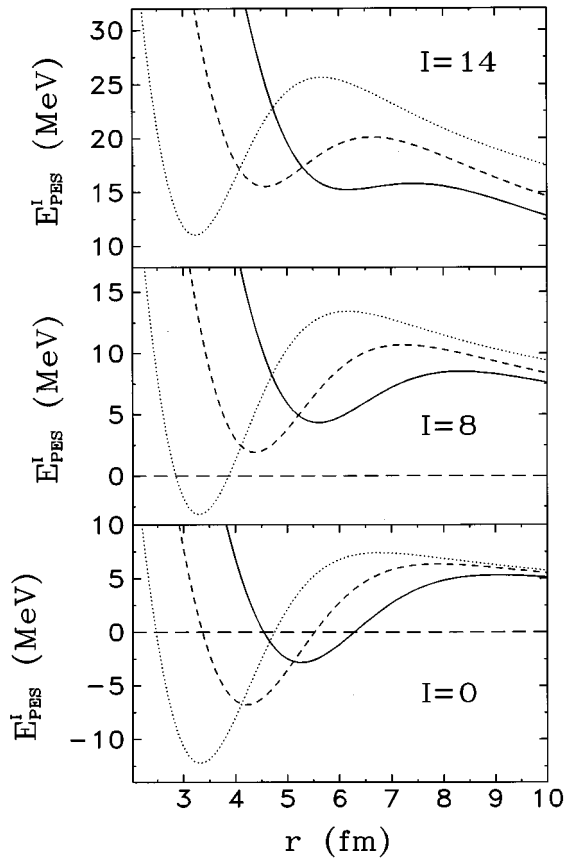

FIG. 3. Radial intersections of the potential energy surfaces for the angular momenta $I=0$, 8, and 14 for three orientations [parallel equator-equator (EE): full; pole-equator (PE): dashed; pole-pole (PP): dotted]. Here, the variables β_1 and β_2 are fixed by their values at the corresponding minimum.

for the pole-pole (PP), the pole-equator (PE), and the parallel equator-equator orientation. The latter means that the symmetry axes of the nuclei are parallel. Each intersection of the PES exhibits a minimum. It is worth mentioning that the potentials without rotational energy are very similar to those of Cugnon *et al.* [25] who have performed constrained Hartree-Fock calculations with a Skyrme S III interaction. Note that the potentials in Fig. 3 are *not* minimal curves except around the minima.

The difference between the internuclear potentials of the orthogonal and parallel EE orientations is roughly 0.25 MeV and the rotational energies differ at most by 0.75 MeV without significantly different coordinates of their minima. Figure 4 shows the molecular potential of butterfly oscillations. It is interesting that there exists a path in the PES of the PE orientation (bottom picture) which allows us to incline the nuclei very much by using only about 1 MeV of energy. In the case of the parallel EE position (upper picture) one can observe elliptic equipotential surfaces lying diagonal which means a preference of touching configurations. On the other hand, the orthogonal EE orientation shows an advantage of independent butterfly oscillations of both nuclei (not illustrated) which is pretty obvious because there does not exist any inclination of the nuclei which increases touching [cf. potential term proportional to C_3 in Eq. (14)]. In Table I we give the minimum energy and the parameters of the PES at

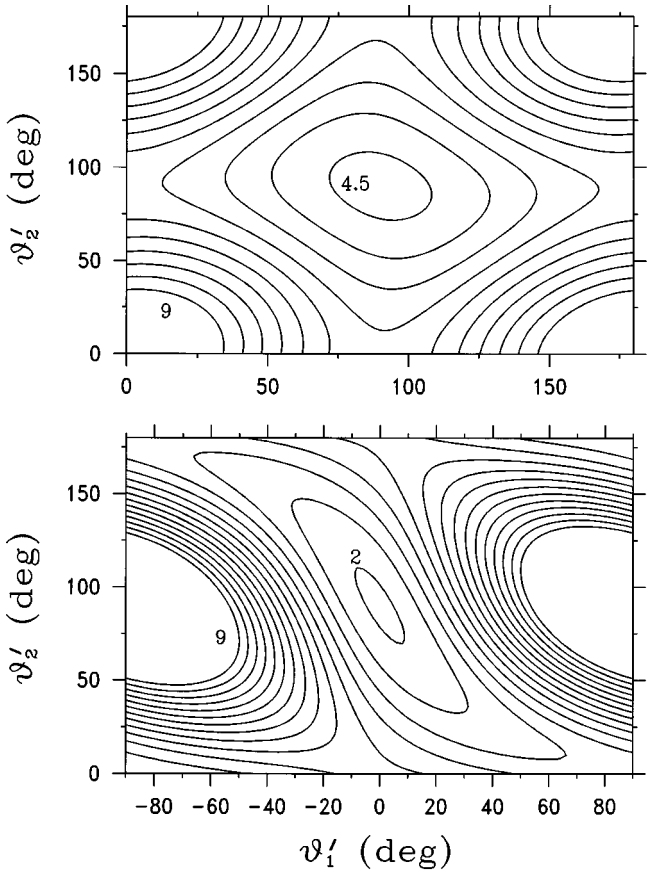

FIG. 4. Potential energy surface for $I=8$ depending on the Euler angles ϑ_1' and ϑ_2' with $\varphi_1'=\varphi_2'=0$ in each case. The remaining variables r,β_1,β_2 are fixed with respect to the minimum of the parallel equator-equator (EE) orientation (upper picture) and with respect to the minimum of the pole-equator (PE) orientation (picture below). The difference between neighboring contour lines is 0.5 MeV.

the potential minima for different angular momenta. C_r, $\tilde{C}_\beta^{(1)}$, and $\tilde{C}_\beta^{(2)}$ are the stiffness parameters of the relative and deformation degrees of freedom, respectively, calculated at the potential minima.

IV. CONSIDERATION OF EQUATOR-EQUATOR-LIKE CONFIGURATIONS

There are some hints that the equator-equator orientation is the most important one for the consideration of molecular resonances [26]. This orientation is connected with maximal elongation and is the first stage of the nuclei brought together with minimized energy. Contrary to this, the pole-pole orientation would be rather connected with fusion and smaller total deformation. So we restrict ourselves in the following to the EE orientation.

A. The Hamiltonian

We assume that motions in the deformation and relative coordinates close to the molecular minima are independent so that a quadratic expansion in these variables can be performed. Besides this, the potential is expanded up to second order in the angles $\tilde{\vartheta}_i'=\vartheta_i'-\pi/2$ $(i=1,2)$:

$$\begin{aligned} V_{\mathrm{EE}}(r,r_0,\xi_1,\xi_2,\varphi_2'-\varphi_1',\tilde{\vartheta}_1',\tilde{\vartheta}_2') &= \frac{C_r}{2}(r-r_0)^2+\frac{\tilde{C}_\beta}{2}\sum_{i=1}^{2}\xi_i^2+V_0+\frac{C_1}{2}(\tilde{\vartheta}_1'^2+\tilde{\vartheta}_2'^2) \\ &+\frac{C_2}{2}\cos[2(\varphi_2'-\varphi_1')](1-\tilde{\vartheta}_1'^2-\tilde{\vartheta}_2'^2) \\ &+\frac{C_3}{2}\cos(\varphi_2'-\varphi_1')\tilde{\vartheta}_1'\tilde{\vartheta}_2'. \end{aligned} \tag{14}$$

The parameters depend on the total angular momentum and are given in Table I and Table II. The coordinates ξ_i are defined as $\xi_i=\beta_i-\tilde{\beta}_0$. By neglecting the γ_i dependences we can write the kinetic part of the Hamiltonian Eq. (1) explicitly as $(\Theta_0=3B_0\tilde{\beta}_0^2)$

TABLE I. The coordinates of the minima and parameters of a harmonic expansion of the effective molecular potential for (a) the parallel equator-equator orientation and (b) the pole-equator orientation.

		$I=0$	$I=2$	$I=4$	$I=6$	$I=8$	$I=10$	$I=12$	$I=14$
(a)	$E_{\min}$ (MeV)	−2.83	−2.17	−0.68	1.53	4.34	7.63	11.29	15.24
	r_0 (fm)	5.27	5.30	5.37	5.47	5.60	5.75	5.93	6.17
	$\tilde{\beta}_0$	−0.58	−0.58	−0.60	−0.62	−0.66	−0.70	−0.73	−0.76
	C_r (MeV fm^{-2})	8.31	8.42	8.10	7.51	6.72	5.79	4.57	2.99
	$\tilde{C}_\beta$ (MeV)	39.6	39.5	38.9	37.4	36.7	37.1	37.4	37.5
(b)	$E_{\min}$ (MeV)	−6.80	−6.03	−4.25	−1.61	1.92	5.86	10.39	15.32
	r_0 (fm)	4.20	4.25	4.35	4.35	4.40	4.45	4.55	4.65
	$\tilde{\beta}_0^{(1)}$	−0.73	−0.74	−0.75	−0.80	−0.83	−0.89	−0.92	−0.95
	$\tilde{\beta}_0^{(2)}$	−0.54	−0.55	−0.58	−0.60	−0.65	−0.69	−0.76	−0.83
	C_r (MeV fm^{-2})	15.0	15.1	13.9	14.0	12.8	13.0	11.7	10.3
	$\tilde{C}_\beta^{(1)}$ (MeV)	45.4	45.4	44.6	44.5	43.7	43.9	43.0	42.2
	$\tilde{C}_\beta^{(2)}$ (MeV)	38.7	38.6	38.2	37.0	34.4	31.5	30.5	32.2

$$T_{\mathrm{EE}}=-\frac{\hbar^2}{2\mu}\frac{1}{r}\frac{\partial^2}{\partial r^2}r-\sum_{i=1}^{2}\frac{\hbar^2}{2B_0}\frac{\partial^2}{\partial\xi_i^2}+\frac{\boldsymbol{I}^2-I_{z'}^2-(J_1)_{z'}^2-(J_2)_{z'}^2}{2\mu r_0^2}+\frac{1}{2}\left(\frac{1}{\Theta_0}+\frac{1}{\mu r_0^2}\right)\sum_{i=1}^{2}\left[(J_i)_{x_i''}^2+(J_i)_{y_i''}^2\right]$$
$$+\frac{1}{\mu r_0^2}\{(J_1)_{x'}(J_2)_{x'}+(J_1)_{y'}(J_2)_{y'}-I_{x'}[(J_1)_{x'}+(J_2)_{x'}]-I_{y'}[(J_1)_{y'}+(J_2)_{y'}]\}. \tag{15}$$

Here the intrinsic angular momentum operators have to be expanded around the EE orientation. In principle, the corresponding Schrödinger equation can now be solved by diagonalization. One can find a basis where most parts of the Hamiltonian $H_{\mathrm{EE}}=T_{\mathrm{EE}}+V_{\mathrm{EE}}$ are diagonal, except for the last two terms in Eq. (14) and the last one in curly brackets in Eq. (15). Since the rotational energy should be roughly the same after diagonalization as in Eq. (12), i.e., it should include individual rotations, one can draw the conclusion that the nondiagonal contributions are anything but small. With the calculation of the nondiagonal matrix elements and the diagonalization of H_{EE} being lengthy, we prefer an approximate method. Instead of using the full form we neglect the last two terms in Eq. (14), which means free rotation of the nuclei in the angle $(\varphi_2'-\varphi_1')$, and rewrite Eq. (15):

$$T_{\mathrm{EE}}=-\frac{\hbar^2}{2\mu}\frac{1}{r}\frac{\partial^2}{\partial r^2}r-\sum_{i=1}^{2}\frac{\hbar^2}{2B_0}\frac{\partial^2}{\partial\xi_i^2}+\frac{\boldsymbol{I}^2-I_{z'}^2}{2(\mu r_0^2+4\Theta_0/3)}$$
$$+\frac{1}{2\Theta_0}\sum_{i=1}^{2}\left[(J_i')_{x_i''}^2+(J_i')_{y_i''}^2\right]. \tag{16}$$

The last two terms in this formula are an approximation and arise from the insertion of

$$(J_i)_{x',y'}=\frac{4\Theta_0/9}{\mu r_0^2+4\Theta_0/3}I_{x',y'}+(J_i')_{x',y'},\quad (J_i)_{z'}=(J_i')_{z'} \tag{17}$$

into Eq. (15), with small terms being neglected and $\mu r_0^2/\Theta_0\approx 6$ (cf. Table I) being used. The rotational energy proportional to $(\boldsymbol{I}^2-I_{z'}^2)$ in Eq. (16) reproduces the rotational energies of Eq. (12) within an error of 0.25 MeV [15]. By measuring the angular momentum of the nuclei with respect to the c.m. system the operators $\boldsymbol{J}_i$ in Eq. (15) yield large contributions to the EE orientation. Therefore, we have introduced the operators $\boldsymbol{J}_i'$ in Eq. (16) which describe the rotation of each nucleus with respect to the MO frame. Here, an exact transformation is difficult to find (for detailed discussion see Ref. [11]).

The intrinsic rotational energy explicitly reads

$$\frac{1}{2\Theta_0}\sum_{i=1}^{2}\left[(J_i')_{x_i''}^2+(J_i')_{y_i''}^2\right]$$
$$=-\frac{\hbar^2}{2\Theta_0}\sum_{i=1}^{2}\left(\frac{\partial^2}{\partial\vartheta_i'^2}+\cot\vartheta_i'\frac{\partial}{\partial\vartheta_i'}+\frac{1}{\sin^2\vartheta_i'}\frac{\partial^2}{\partial\varphi_i'^2}\right). \tag{18}$$

Transforming the volume element from $d\varphi_1'd\varphi_2'\times\sin\vartheta_1'd\vartheta_1'\sin\vartheta_2'd\vartheta_2'r^2drd\Omega d\xi_1d\xi_2$ to $d\varphi_1'd\varphi_2'd\vartheta_1'd\vartheta_2'r^2\times drd\Omega d\xi_1d\xi_2$ yields a change of the differential operators in ϑ_i':

$$-\frac{\hbar^2}{2\Theta_0}\sqrt{\sin\vartheta_i'}\left(\frac{\partial^2}{\partial\vartheta_i'^2}+\cot\vartheta_i'\frac{\partial}{\partial\vartheta_i'}\right)\frac{1}{\sqrt{\sin\vartheta_i'}}$$
$$=-\frac{\hbar^2}{2\Theta_0}\left(\frac{\partial^2}{\partial\vartheta_i'^2}+\frac{1}{4}\cot^2\vartheta_i'+\frac{1}{2}\right). \tag{19}$$

Expanding the approximate Hamiltonian up to second order in $\tilde{\vartheta}_1'$ and $\tilde{\vartheta}_2'$ we finally get

$$\tilde{H}_{\mathrm{EE}}=-\frac{\hbar^2}{2\mu}\frac{1}{r}\frac{\partial^2}{\partial r^2}r-\frac{\hbar^2}{2B_0}\left(\frac{\partial^2}{\partial\xi_+^2}+\frac{\partial^2}{\partial\xi_-^2}\right)+\frac{\boldsymbol{I}^2-I_{z'}^2}{2(\mu r_0^2+4\Theta_0/3)}-\frac{\hbar^2}{2\Theta_0}\sum_{i=1}^{2}\left[\frac{\partial^2}{\partial\tilde{\vartheta}_i'^2}+(1+\tilde{\vartheta}_i'^2)\frac{\partial^2}{\partial\varphi_i'^2}\right]+\frac{C_r}{2}(r-r_0)^2$$
$$+\frac{\tilde{C}_\beta}{2}(\xi_+^2+\xi_-^2)+\frac{1}{2}\left(C_1-\frac{\hbar^2}{4\Theta_0}\right)(\tilde{\vartheta}_1'^2+\tilde{\vartheta}_2'^2)+V_0-\frac{\hbar^2}{2\Theta_0}. \tag{20}$$

TABLE II. The coefficients of the potential expansion (in MeV) in the Euler angles $\tilde{\vartheta}_i$ around the EE orientation [see Eq. (14)].

	$I=0$	$I=2$	$I=4$	$I=6$	$I=8$	$I=10$	$I=12$	$I=14$
V_0	−2.71	−2.70	−2.65	−2.52	−2.19	−1.64	−0.92	0.16
C_1	0.55	0.91	1.68	2.72	3.96	5.22	6.36	7.26
C_2	−0.25	−0.25	−0.26	−0.26	−0.27	−0.27	−0.25	−0.22
C_3	0.41	0.60	1.08	1.69	2.48	3.23	3.79	4.09

For reasons of symmetrization in the next section, we have introduced the coordinates $\xi_\pm = 2^{-1/2}(\xi_1 \pm \xi_2)$ in Eq. (20). Note that the corresponding wave functions have to be used with the simplified volume element.

B. Eigenstates of the approximate Hamiltonian

In order to solve the Schrödinger equation for the EE orientation we make the following ansatz:

$$\Psi_\nu(r,\Omega,\Omega_1',\Omega_2',\xi_+,\xi_-) = R_\nu(r) S |\nu\rangle, \tag{21a}$$

$$|\nu\rangle = \left(\frac{2I+1}{8\pi^2}\right)^{1/2} D^{I*}_{MK}(\Omega)\,\Xi_\alpha(\Omega_1',\Omega_2')\,v_{\mu_+}(\xi_+)\,v_{\mu_-}(\xi_-), \tag{21b}$$

where S is a symmetrization operator including the normalization. The Schrödinger equation separates into four differential equations. The equations depending on ξ_+ and ξ_- can be simply solved by normalized one-dimensional harmonic oscillator eigenfunctions $v_{\mu_+}(\xi_+)$ and $v_{\mu_-}(\xi_-)$, respectively ($\mu_+, \mu_- = 0,1,2,\ldots$). By additionally substituting $R_\nu(r) = g(r-r_0)/r$, the solution $g(r-r_0)$ of the corresponding third differential equation is a harmonic oscillator eigenfunction, too. The remaining equation reads as follows:

$$\left\{ \frac{-\hbar^2}{2\Theta_0} \sum_{i=1}^{2} \left[\frac{\partial^2}{\partial \tilde{\vartheta}_i'^2} + (1+\tilde{\vartheta}_i'^2) \frac{\partial^2}{\partial \varphi_i'^2} \right] + \frac{1}{2}\left(C_1 - \frac{\hbar^2}{4\Theta_0} \right) \sum_{i=1}^{2} \tilde{\vartheta}_i'^2 - E_\alpha \right\} \Xi_\alpha(\Omega_1',\Omega_2') = 0. \tag{22}$$

This equation has the solution

$$\Xi_\alpha(\Omega_1',\Omega_2') = \frac{1}{4\pi^2} \exp(ik_1\varphi_1') \exp(ik_2\varphi_2') \times \Phi_{n_1|k_1|}(\tilde{\vartheta}_1') \Phi_{n_2|k_2|}(\tilde{\vartheta}_2'). \tag{23}$$

Here an integration in the ψ_i' coordinate is provided [normalization constant $(2\pi)^{-1}$] analogously to the channel wave functions. The functions $\Phi_{n_i|k_i|}(\tilde{\vartheta}_i')$ are harmonic oscillator eigenfunctions which additionally depend on the rotational quantum numbers k_i $(i=1,2)$

$$\Phi_{n_i|k_i|} = N_{n_i} H_{n_i}(\alpha_i \tilde{\vartheta}_i') \exp(-\alpha_i^2 \tilde{\vartheta}_i'^2/2), \tag{24}$$

with

$$\alpha_i = \left(\frac{C_1\Theta_0}{\hbar^2} + k_i^2 - \frac{1}{4} \right)^{1/4}, \quad N_{n_i} = \left(\frac{\alpha_i}{\sqrt{\pi} 2^{n_i} n_i!} \right)^{1/2}. \tag{25}$$

$H_{n_i}(x)$ denotes a Hermite polynomial. The demand for periodicity with 2π in the angles φ_1' and φ_2' restrict the quantum numbers k_1 and k_2 to integers. As the wave function Ψ_ν has to fulfill the condition $[I_{z'} - (J_1')_{z'} - (J_2')_{z'}]\Psi_\nu = 0$ [11], we have $k_1 + k_2 = K$. Introducing the quantum number $\kappa = k_1 - k_2$ for the asymmetric rotational mode around the molecular z' axis, we can replace the quantum numbers k_1 and k_2 by $K = k_1 + k_2$ and $\kappa = k_1 - k_2$ in the following.

The operator S in Eq. (21) symmetrizes the wave function with respect to an inversion of the intrinsic z_i'' axes, an exchange of the nuclei and a parity operation ($\boldsymbol{r} \to -\boldsymbol{r}$). Then, the wave function should be invariant under the inversion of the intrinsic z_i'' axes:

$$\tilde{\vartheta}_i' \to -\tilde{\vartheta}_i', \quad \varphi_i' \to \varphi_i' + \pi \quad (i=1,2). \tag{26}$$

It can be seen that the wave function $\Xi_\alpha(\Omega_1',\Omega_2')$ is a eigenfunction of these symmetry operations with the eigenvalues $(-)^{k_i+n_i}$. Thus choosing those wave functions with positive eigenvalues leads to the rule

$$k_1 + n_1 \text{: even} \ \wedge \ k_2 + n_2 \text{: even}. \tag{27}$$

Here, this symmetrization reduces the number of solutions, in contrast to the case of the ^{24}Mg + ^{24}Mg system.

The exchange of both identical nuclei changes the wave function in the following manner:

$$|\nu = (I,M,K,\kappa,n_1,n_2,\mu_+,\mu_-)\rangle \to (-)^{I+\mu_-+n_1+n_2} \times |\nu = (I,M,-K,\kappa,n_2,n_1,\mu_+,\mu_-)\rangle. \tag{28}$$

Analogously, the global parity operation ($\boldsymbol{r} \to -\boldsymbol{r}$) yields

$$|\nu = (I,M,K,\kappa,n_1,n_2,\mu_+,\mu_-)\rangle \to (-)^{I+n_1+n_2} \times |\nu = (I,M,-K,-\kappa,n_1,n_2,\mu_+,\mu_-)\rangle. \tag{29}$$

As the elastic and inelastic channel wave functions have positive parity we choose the same paritiy for the quasibound states. Otherwise, there is no overlap between both types of wave functions. By additionally using the relation $(-)^{n_1+n_2} = (-)^K$ which holds due to Eq. (27) the symmetrized wave function can be written as

$$S|\nu\rangle = N_\nu[|\nu = (I,M,K,\kappa,n_1,n_2,\mu_+,\mu_-)\rangle + (-)^{I+K+\mu_-}|\nu = (I,M,-K,\kappa,n_2,n_1,\mu_+,\mu_-)\rangle + (-)^{I+K}|\nu = (I,M,-K,-\kappa,n_1,n_2,\mu_+,\mu_-)\rangle + (-)^{\mu_-}|\nu = (I,M,K,-\kappa,n_2,n_1,\mu_+,\mu_-)\rangle], \tag{30}$$

TABLE III. The energy constants used in Eq. (35) for angular momenta $I=0$ to $I=14$ in MeV. The values of $\hbar\omega_{\vartheta_i}$ are given for different quantum numbers of $|k_i|$.

	$I=0$	$I=2$	$I=4$	$I=6$	$I=8$	$I=10$	$I=12$	$I=14$
D_K	0.292	0.302	0.271	0.251	0.216	0.188	0.172	0.158
D_κ	0.396	0.396	0.370	0.347	0.306	0.272	0.250	0.231
$\hbar\omega_{\vartheta_i}(\|k_i\|=0)$	0.494	0.906	1.390	1.815	2.115	2.319	2.472	2.547
$\hbar\omega_{\vartheta_i}(\|k_i\|=1)$	1.658	1.825	2.030	2.284	2.444	2.562	2.667	2.709
$\hbar\omega_{\vartheta_i}(\|k_i\|=2)$	3.204	3.296	3.270	3.313	3.234	3.179	3.180	3.145
$\hbar\omega_\beta$	7.95	7.95	7.88	7.73	7.66	7.70	7.74	7.74
$\hbar\omega_r$	7.61	7.66	7.51	7.23	6.84	6.35	5.64	4.56

with

$$N_\nu=\frac{1}{2}\{1+(-)^I\delta_{K0}\delta_{\kappa 0}+(-)^{\mu_-}\delta_{n_1n_2}[\delta_{\kappa 0}+(-)^I\delta_{K0}]\}^{-1/2}. \tag{31}$$

With the total angular momentum being even in the scattering of two bosonic nuclei with spin zero, the following selection rules can be summed up:

$$(K+\kappa)/2+n_1\text{: even}, \quad (K-\kappa)/2+n_2\text{: even},$$

$$K\pm\kappa\text{: even}, \quad K\geqslant 0,$$

$$\kappa\geqslant 0 \text{ for } (n_1=n_2)\vee(K=0), \quad n_1\geqslant n_2,$$

$$\mu_-\text{: even for } (n_1=n_2)\wedge[(\kappa=0)\vee(K=0)]. \tag{32}$$

Combined with these rules the eigenenergies can be calculated by means of the formula

$$\begin{aligned}E_\nu=E_{IK\kappa n_1n_2n_r\mu_+\mu_-}&=\tilde{E}_0(I)+D_KK^2+D_\kappa(\kappa^2-2)\\&+\hbar\omega_r(n_r+1/2)+\hbar\omega_{\vartheta_1}(n_1+1/2)+\hbar\omega_{\vartheta_2}(n_2+1/2)\\&+\hbar\omega_\beta(\mu_++\mu_-),\end{aligned} \tag{33}$$

with

$$\tilde{E}_0(I)=V_0+\frac{[I(I+1)]\hbar^2}{2(\mu r_0^2+4\Theta_0/3)}. \tag{34}$$

The quantities D_K and D_κ and frequencies are given as

$$D_K=\hbar^2[(2\Theta_0)^{-1}-(\mu r_0^2+4\Theta_0/3)^{-1}]/2,$$

$$D_\kappa=\hbar^2/(4\Theta_0),$$

$$\omega_{\vartheta_1}=\{C_1/\Theta_0+\hbar^2[(K+\kappa)^2-1]/(4\Theta_0^2)\}^{1/2},$$

$$\omega_{\vartheta_2}=\{C_1/\Theta_0+\hbar^2[(K-\kappa)^2-1]/(4\Theta_0^2)\}^{1/2},$$

$$\omega_r=(C_r/\mu)^{1/2}, \quad \omega_\beta=(\tilde{C}_\beta/B_0)^{1/2}. \tag{35}$$

For the β vibrations the zero-point energies are not included because the asymptotic potential energy ($r\to\infty$) is just defined with respect to the vibrational ground state of each nucleus and these vibrational zero-point energies do not change much with the relative distance. The other degrees of freedom have zero-point energies.

Table III gives the values of D_K, D_κ and of the vibrational energies for different angular momenta. Calculated energies of resonances are shown for $I=8$ in Fig. 5 and are listed for $I=4$, 10, and 14 in Table IV. As in the work of Refs. [9,14] there exists the mode of simultaneous rotation (K mode) and the one of opposite rotation (κ mode) of both nuclei around the z' axis. Together with the butterfly modes they build up the low energy spectrum of the molecule. Here, the butterfly modes are independent vibrations of each nucleus because the responsible coupling terms in the potential have been just neglected (cf. Sec. III B). On raising I one can observe an increasing stiffness of the lowest butterfly potential, whereas the rotational energy decreases. It is interesting to compare our butterfly frequencies to those of Hess and Pereyra [27] who have used parameters of an energy formula fitted to the experimental spectrum of $I=0$. They have obtained a butterfly excitation energy of 1.13 MeV to which our values of small I are very close. Moreover, the β_i degrees of freedom apparently do not need to be especially considered since the excitation energy of surface vi-

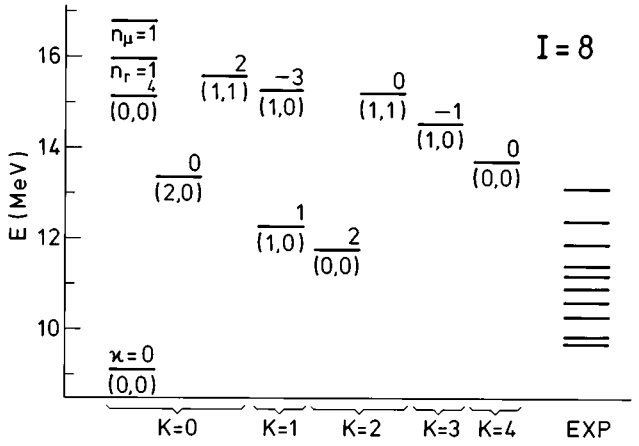

FIG. 5. Energies of the quasibound states for the $^{12}C+{}^{12}C$ system around the parallel equator-equator orientation for an angular momentum $I=8$. Only energies up to 17 MeV are given. For each state the quantum numbers K, κ (number above the lines), n_1 and n_2 ((n_1,n_2) = numbers below the lines) are shown, the other ones are set zero with exception of the first excited states with $n_r=1$ and $\mu_+=1$. The levels are ordered according to the scheme of Uegaki and Abe [14]. The experimental resonance energies are taken from Abbondanno [28].

TABLE IV. Molecular excitation energy (in MeV) and summed partial widths (in keV) for the decay of the molecular state $\nu=(I,\tilde{\nu})=(I,K,\kappa,n_1,n_2,n_r,\mu_+,\mu_-)$ into a scattering state $(J_1^{\pi_1},J_2^{\pi_2})$, the angular momenta $I=4$, 10, and 14 being chosen as representative examples. The summation of widths runs over all possible decay channels c leading to the given final state. In parentheses the summed reduced widths (in % of $\gamma_{\rm sp}^2$) calculated with the Coulomb penetrability of the stretched configuration ($\ell_c=I-J_1-J_2$) are given. The brackets in the second column mean (K,κ,n_1,n_2), and an asterisk denotes $n_r=1$, otherwise $n_r=0$. The remaining quantum numbers are zero.

			Widths							
I	$\tilde{\nu}$	E_ν	$(0^+,0^+)$		$(2^+,0^+)$		$(2^+,2^+)$		$(4^+,0^+)$	
4	g.s.	3.74	0.0	(16.58)	0.0	(0.00)	0.0	(0.00)		
	(0,0,2,0)	6.53	1.4	(0.78)	0.0	(1.60)	0.0	(0.00)		
	(1,1,1,0)	6.73	—		0.0	(2.51)	0.0	(0.00)		
	(2,2,0,0)	7.24	—		0.0	(1.71)	0.0	(0.00)		
	(0,0,2,2)	9.31	0.1	(0.01)	0.0	(0.08)	0.0	(0.31)		
	(0,0,4,0)	9.31	10.3	(0.66)	0.4	(1.85)	0.0	(0.00)		
	(1,−1,2,1)	9.52	—		0.0	(0.06)	0.0	(0.95)		
	(2,0,1,1)	9.53	—		—		0.0	(0.63)		
	(3,−1,1,0)	9.84	—		—		0.0	(1.17)		
	(0,2,1,1)	9.92	—		—		0.0	(0.27)		
	(4,0,0,0)	9.95	—		—		0.0	(1.53)		
	(2,−2,2,0)	10.03	—		0.1	(0.05)	0.0	(0.56)		
	(1,−3,1,0)	10.63	—		—		0.0	(0.33)		
	(1,1,3,0)	10.80	—		4.1	(1.14)	0.0	(0.00)		
	(0,0,0,0)*	11.26	1984.2	(77.06)	0.2	(0.04)	0.0	(0.00)		
10	g.s.	12.52	196.1	(29.92)	0.3	(0.45)	0.0	(0.00)		
	(2,2,0,0)	14.79	—		14.5	(2.29)	0.0	(0.02)		
	(1,1,1,0)	15.66	—		40.7	(4.01)	0.0	(0.06)		
	(4,0,0,0)	16.39	—		—		0.3	(0.17)		
	(0,0,2,0)	17.16	120.8	(4.67)	47.1	(2.73)	0.2	(0.05)		
	(3,−1,1,0)	17.60	—		—		2.6	(0.41)		
	(0,4,0,0)	17.73	—		—		0.9	(0.12)		
	(1,−3,1,0)	18.26	—		—		3.5	(0.36)		
	(2,0,1,1)	18.64	—		—		4.8	(0.41)		
	(0,0,0,0)*	18.87	3021.9	(93.67)	50.2	(2.01)	0.1	(0.01)		
	(0,2,1,1)	18.97	—		—		4.6	(0.35)		
	(2,−2,2,0)	19.43	—		9.4	(0.34)	5.8	(0.37)		
	(1,−1,2,1)	20.30	—		11.3	(0.37)	16.3	(0.81)		
14	g.s.	19.72	582.7	(37.75)	11.1	(1.09)	0.0	(0.01)	0.0	(0.00)
	(2,2,0,0)	21.57	—		71.2	(4.08)	0.5	(0.05)	0.0	(0.00)
	(4,0,0,0)	22.85	—		—		6.3	(0.41)	—	
	(1,1,1,0)	22.90	—		122.5	(5.42)	2.2	(0.14)	0.0	(0.02)
	(0,4,0,0)	24.01	—		—		7.5	(0.37)	—	
	(0,0,0,0)*	24.29	2476.2	(78.91)	81.9	(2.96)	0.5	(0.02)	0.0	(0.01)
	(3,−1,1,0)	24.46	—		—		16.3	(0.74)	—	
	(0,0,2,0)	24.81	357.5	(10.83)	92.1	(3.13)	3.3	(0.14)	0.4	(0.12)
	(1,−3,1,0)	25.04	—		—		17.9	(0.74)	—	
	(2,0,1,1)	25.93	—		—		20.5	(0.74)	—	
	(2,2,0,0)*	26.14	—		431.7	(12.77)	5.8	(0.20)	0.1	(0.01)
	(0,2,1,1)	26.22	—		—		20.6	(0.71)	—	
	(2,−2,2,0)	26.67	—		31.9	(0.90)	19.0	(0.62)	0.0	(0.00)
	(4,4,0,0)	26.91	—		—		—		7.6	(0.73)

brations is nearly identical to the corresponding value of an isolated nucleus. But the β_i variables must not be fixed because the individual moments of inertia considerably depend on them (cf. Table I).

Theoretical and experimental resonances are compared in Fig. 6. It is remarkable that, in most cases, the theory reproduces the experimental level density at higher energies. The absolute location of the theoretical spectrum depends on the

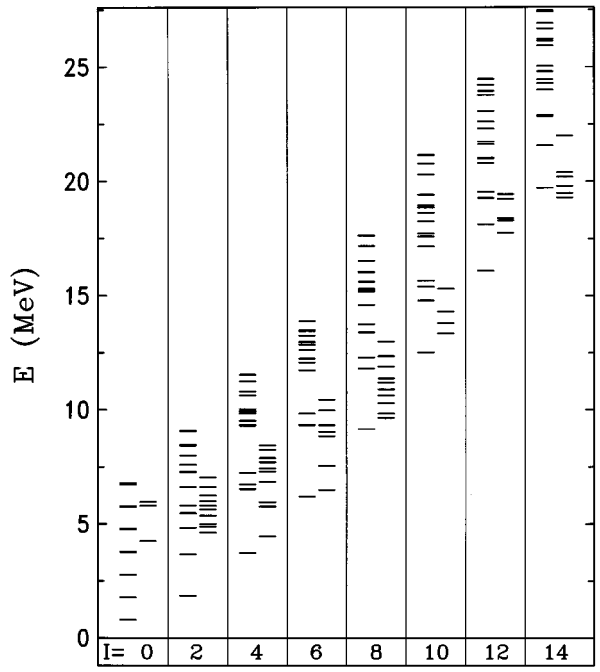

FIG. 6. Calculated and experimental resonance energies for various angular momenta. The calculated energies (left-hand side of each column) are the eigenenergies for the equator-equator orientation of the ^{12}C nuclei. The experimental data (right-hand side of each column) are taken from Abbondanno [28].

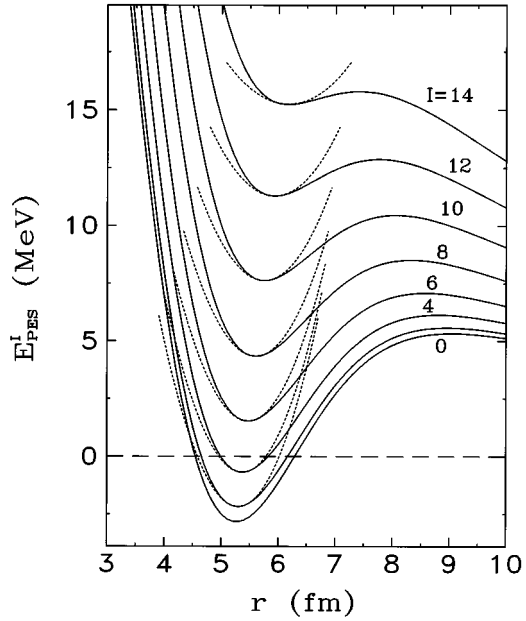

FIG. 7. Harmonic approximation of the molecular potential in the radial coordinate for different values of total angular momentum (dotted lines) around the corresponding minimum. The right edge of each parabola denotes the cutoff at the channel radius $a(I)$.

shape and height of the real potential. As stated above, this potential was obtained by fitting its parameters to the elastic ^{12}C+^{12}C scattering. Apagyi *et al.* [29] recently solved the inverse scattering problem with experimental ^{12}C+^{12}C elastic scattering data and got energy-dependent potentials with different shapes. Comparing our real potential with those of Apagyi *et al.* [29] we conclude that it is difficult to fix the absolute energy of the resonances without an experimental evidence for a special resonance state. However, the relative positions of the resonances as a function of the angular momentum I are not very sensitive on the real potential. The slopes of both the deformation coordinate $\tilde{\beta}_0(I)$ and the radial stiffness $C_r(I)$ with respect to I are nearly independent of the potential parameters and consequently, the slopes of the functions $D_K(I), D_\kappa(I), \omega_{\vartheta_i}(I)$, and $\omega_r(I)$ have the same property. Therefore, the relative position of the resonance energies resulted nearly quantitatively, if we had not introduced several simplifications in our model. The effects of these simplifications will be studied next.

It is clear that our calculations are based on a simplified model for the rotation and oscillations of the ^{12}C+^{12}C system with special assumptions for the dynamics and parameters based on realistic physical grounds. Therefore, our model can only give a qualitative description of the resonance states, but not a quantitative prediction of their absolute energies.

C. The decay widths

For the calculation of widths we use the R-matrix theory. Here the molecular state Ψ_ν is regarded as a member of a complete set of orthogonal basis states inside the spherical nuclear interaction region $0 \leqslant r \leqslant a$ (interior region in R-matrix theory). Accordingly, the decay of Ψ_ν into the channel $|c\rangle$ has a partial width defined as

$$\Gamma_{\nu c} = 2 P_c(k_c a)\, \gamma_{\nu c}^2 \tag{36}$$

with the Coulomb penetrability

$$P_c(k_c a) = k_c a / [G_{l_c}(k_c a)^2 + F_{l_c}(k_c a)^2]. \tag{37}$$

The reduced partial width

$$\gamma_{\nu c}^2 = \frac{\hbar^2}{2\mu} a R_\nu(a)^2 |\langle c | \nu \rangle|^2 \tag{38}$$

in Eq. (36) is commonly given in terms of the so-called Wigner-Teichmann single-particle limit:

$$\gamma_{\rm sp}^2 = \frac{3}{a} \frac{\hbar^2}{2\mu}. \tag{39}$$

On calculating the scalar product we have used the volume element $d\Omega_1' d\Omega_2' \ldots$ and have divided the molecular wave function by $(\sin\vartheta_1' \sin\vartheta_2')^{1/2}$. The channel radius a is important due to our bound state approximation and should roughly describe the location of the actual potential barrier. Since formulas applied, e.g., to ^{24}Mg + ^{24}Mg do not match this condition here, we have estimated the channel radius visually [the right ends of the dotted parabolas in Fig. 7 indicate the used channel radii $a(I)$]. Summed partial widths of the lowest molecular states for selected angular momenta are given in Table IV. Here a dash denotes zero overlap of the wave functions and thus a vanishing width per construc-

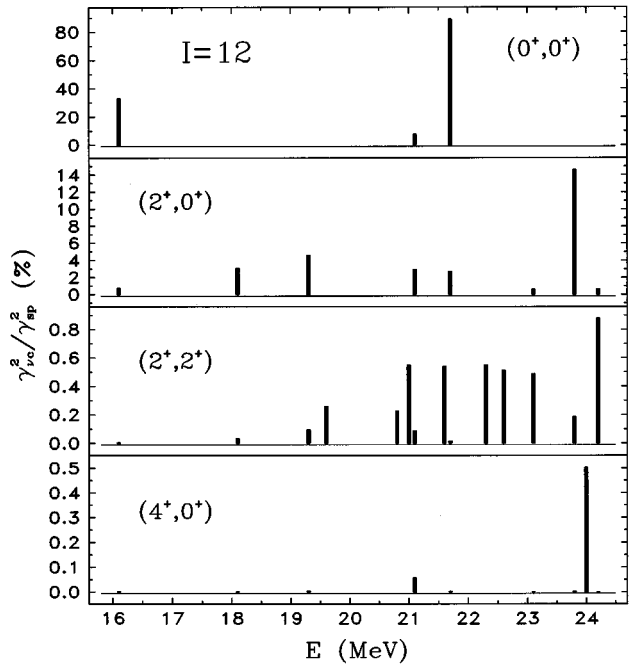

FIG. 8. The summed reduced widths in terms of the Wigner-Teichmann single-particle limit for $I=12$ and different final states. For explanation see caption of Table IV.

tionem. In parentheses the summed reduced widths are given, shown additionally for $I=12$ in Fig. 8.

The Coulomb penetrability strongly increases with k_c being calculated by means of $\hbar^2 k_c^2/2\mu = E_\nu - E_{\rm exc}$. Therefore, the higher the excitation energy of the final state is, the more the widths of the decay into the corresponding channels are diminished. However, the summed reduced widths, which should not depend on $P_c(k_c a)$ anymore, show the same dependency. So an inspection of $|\langle c|\nu\rangle|$ reveals that this overlap lies inside the interval of 0.25 and 1.00 for elastic widths with $K=\kappa=0$, each molecular ground state having nearly full overlap with the elastic channel wave function. In the case of the $(2^+,0^+)$ final state the scalar products vary around 0.10 and those of the mutually excited final state are even smaller. Variations of the molecular potential within realistic ranges do not change this dependency very much; above all the nonvanishing elastic overlaps are fairly stable. Only the magnitudes of the calculated widths are more sensitive to such variations due to their shifted resonance energies. Despite this, the mutual relations of the widths of the resonances are nearly conserved. It is noticeable that the first excited states in the radial potential $(n_r=1)$ have elastic widths of 2 to 3 MeV since these states lie considerably above the Coulomb barrier and are no more bound.

In our approximations many quasibound states have no overlap with the elastic entrance channel. This deficiency could be removed by a diagonalization of the complete Hamiltonian which would lead to states which all have small overlaps with the elastic entrance channel. Such calculations are planned for the near future. Presently we cannot compare our calculated widths quantitatively with the experimental ones, but the gross tendency of the widths is very similar to the experimental ones.

V. SUMMARY

For the interpretation of the resonances in the scattering of two oblately deformed ^{12}C nuclei, we have used a molecular model which has been originally developed and successfully applied to the case of two prolately deformed nuclei. We have shown that the formation of dinuclear ^{24}Mg configurations consisting of two oblate ^{12}C nuclei in equator-equator orientation can cause intermediate resonances in the ^{12}C + ^{12}C scattering. Here, mainly the Pauli principle, incorporated phenomenologically, prevents the nuclei from fusing. Characteristic of the treated equator-equator orientation are the maximal elongation and the minimal height of the Coulomb barrier.

Starting with a double-folding potential, we have added the rotational energy of a stiff molecular rotator and performed an expansion of the potential around the equator-equator orientation. By simplifying complicated terms in the Hamiltonian we have calculated a spectrum of resonances revealing about two states per MeV. The low energy spectrum is dominated by rotations of the nuclei around the z'-axis and butterfly oscillations. Although surface vibrations of the nuclei in the molecule have small importance, the β_i degrees of freedom must not be fixed because of the sensitive influence upon the intrinsic moments of inertia.

The decay widths of the molecular states into selected ^{12}C channels show the experimental characteristics at an average, but for a detailed comparison the Hamiltonian should be diagonalized. As we have used a bound state approximation with the nuclei strongly inclined, one can draw the conclusion that, furthermore, the radial and butterfly modes are actually strongly coupled.

Since the model for the resonance states is phenomenological and includes several simplifications for the dynamics like the linearization of the oscillations and the free rotation of the nuclei around the internuclear axis, we conclude that the resulting energies of the quasibound states should be understood as qualitative values. Comparison with experimental resonances in the ^{12}C+^{12}C system yields the right order of level density. Nevertheless one has to keep in mind that not all the experimental resonances belong to states in the equator-equator orientation, but may also be described with configurations consisting of more than two clusters. The physical nature of the experimental resonances is not well understood with the exception of the virtual resonances with large widths in the nucleus-nucleus potentials. Therefore, it is nearly impossible to compare calculated resonances directly and quantitatively with measured resonances; only certain predictions can be stated about the level density of the resonance states above the energy of the lowest state for each angular momentum.

ACKNOWLEDGMENTS

We are indebted to Professor P.O. Hess, Professor U. Mosel, and Dr. E. Uegaki for useful discussions. This work was supported by BMFT(06 GI 728) and Gesellschaft für Schwerionenforschung (Darmstadt).

[1] D.A. Bromley, J.A. Kühner, and E. Almquist, Phys. Rev. Lett. **4**, 365 (1960).
[2] R. Stokstad, D. Shapira, L. Chua, P. Parker, M.W. Sachs, R. Wieland, and D.A. Bromley, Phys. Rev. Lett. **28**, 1523 (1972).
[3] R.W. Zurmühle, P. Kutt, R.R. Betts, S. Saini, F. Haas, and O. Hansen, Phys. Rev. B **129**, 384 (1983).
[4] R.R. Betts, B.B. Back, and B.G. Glagola, Phys. Rev. Lett. **47**, 23 (1981).
[5] G. Gaul and W. Bickel, Phys. Rev. C **34**, 326 (1986).
[6] R.F.A. Hoernle and J.P.F. Sellschop, J. Phys. G **13**, 213 (1987).
[7] W. Greiner, J.Y. Park, and W. Scheid, *Nuclear Molecules* (World Scientific Pub, Singapore, 1995).
[8] E. Uegaki and Y. Abe, Phys. Lett. B **231**, 28 (1989).
[9] E. Uegaki and Y. Abe, Prog. Theor. Phys. **90**, 615 (1993).
[10] R. Maass and W. Scheid, Phys. Lett. B **202**, 26 (1988).
[11] R. Maass and W. Scheid, J. Phys. G **16**, 1359 (1990).
[12] R. Maass and W. Scheid, J. Phys. G **18**, 707 (1992).
[13] R. Könnecke, J. Guirguis, W. Greiner, and W. Scheid, J. Phys. G **8**, 535 (1982).
[14] E. Uegaki and Y. Abe, Phys. Lett. B **340**, 143 (1994).
[15] J. Schmidt, Diploma thesis, Universität Giessen, 1993.
[16] J.M. Eisenberg and W. Greiner, *Nuclear Theory*, 3rd ed., Nuclear Models Vol. 1 (North-Holland, Amsterdam, 1987).
[17] P.O. Hess, J. Schmidt, and W. Scheid, Ann. Phys. (N.Y.) **240**, 22 (1995).
[18] G.R. Satchler and W.G. Love, Phys. Rev. **55**, 183 (1979).
[19] G.R. Satchler, *Direct Nuclear Reactions* (Clarendon Press, Oxford, 1983).
[20] K.W. Jones *et al.*, Phys. Rev. C **33** 17 (1986).
[21] Y. Abgrall, B. Morand, and E. Caurier, Nucl. Phys. A **192**, 372 (1972).
[22] R.H. Helm, Phys. Rev. **104**, 1466 (1956).
[23] G. Helling, W. Scheid, and W. Greiner, Phys. Lett. **36B**, 64 (1971).
[24] S.K. Korotky, Ph.D. thesis, Yale University, 1980.
[25] J. Cugnon, H. Coubre, and H. Flocard, Nucl. Phys. A **331**, 213 (1979).
[26] O. Tanimura and T. Tazawa, Phys. Lett. **78B**, 1 (1978).
[27] P.O. Hess and P. Pereyra, Phys. Rev. C **42**, 1632 (1990).
[28] U. Abbondanno, *A Collection of Data on Resonances in Heavy Ion Reactions* (Istituto Nazionale di Fisica Nucleare, Sezione di Trieste, Trieste, 1991).
[29] B. Apagyi, A. Schmidt, W. Scheid, and H. Voit, Phys. Rev. C **49**, 2608 (1994).